Effects of Thermal Variations on the Tensile Behavior of FRCM Strengthening Systems

Francesca Ferretti[1]; Anna Rosa Tilocca[2]; Andrea Incerti[3]; Claudio Mazzotti[4]; and Marco Savoia[5]

Abstract: Use of fabric-reinforced cementitious matrices (FRCM) is a very efficient strengthening solution for improving the structural behavior of existing masonry elements. FRCM are capable of improving the load-bearing capacity of masonry panels, at the same time providing more ductile behavior. However, the mechanical performances of these materials could be significantly affected by environmental conditions, such as exposure to thermal variations. This aspect should be properly assessed by guidelines and standards devoted to the design of strengthening interventions. Within this framework, the objective of the present research was to evaluate the effect of a temperature increase on the tensile behavior of various FRCM systems, composed of steel, basalt, or aramid-glass fibers and lime-based or cement-based mortar matrices. Tensile tests were performed for each system under different thermal conditioning protocols, comprising different target temperatures, exposure periods, test conditions, and adopted heating sources. The test results showed that the effect of temperature is more evident in the first phases of the tensile tests, that is, during the uncracked phase and the mortar matrix cracking phase, whereas it is less significant in the final phase, which was more related to fiber behavior. Comparisons between the different thermal conditioning procedures are critically discussed within the paper and, in light of the results obtained, recommendations are included to optimize the testing procedures for future research and qualification procedures. **DOI: 10.1061/(ASCE)CC.1943-5614.0001241**.

Author keywords: FRCM; SRG; Tensile behavior; Thermal variations; Thermal conditioning.

Introduction

Since the seismic vulnerability of masonry buildings is a critical issue in the framework of safety assessments of existing constructions (Ceci et al. 2010; Del Gaudio et al. 2021; Lagomarsino 2006; Penna 2015), the use of composite materials for structural retrofitting has rapidly increased in recent years due to their effectiveness in improving survivability in the event of an earthquake (Alecci et al. 2019; Incerti et al. 2015; Shrive 2006; Valluzzi 2016). In particular, fabric-reinforced cementitious matrices (FRCM) systems are adopted nowadays as an efficient strengthening solution for improving of the structural behavior of masonry elements, those both subjected to in-plane and out-of-plane actions (Mininno et al. 2017). Indeed, they are capable of increasing the load-bearing capacity of masonry panels providing, at the same time, more ductile behavior. Significant research, from experimental and numerical points of view, has been devoted to the study of both tensile and bond behavior of a great variety of FRCM systems (Ascione et al. 2015; Bellini et al. 2019a, b; Carozzi et al. 2017; Ceroni et al. 2014; de Felice et al. 2016; Lignola et al. 2017; Valluzzi et al. 2012), as well as to the analysis of the in-plane (Babaeidarabad et al. 2014; Ferretti and Mazzotti 2021; Incerti et al. 2019; Murgo et al. 2021; Del Zoppo et al. 2019) and out-of-plane (Bellini et al. 2018; D'Ambra et al. 2019; Papanicolaou et al. 2007) behavior of full-scale strengthened masonry walls. In these researches, various masonry typologies, FRCM systems, and reinforcing layouts were investigated, confirming that FRCM can be a profitable and suitable strengthening solution (Faella et al. 2010; Ferretti et al. 2021; Marcari et al. 2017; Oliveira et al. 2012; Parisi et al. 2013), when compared with other more traditional techniques.

A critical issue to be considered for a comprehensive definition of the effectiveness of FRCM systems is their durability. For this purpose, several studies concerning the behavior of these composite materials when exposed to aggressive environments have been conducted in recent years, showing how such conditions can affect the performance of FRCM systems (Bellini et al. 2020; Dalalbashi et al. 2021; Donnini 2019; Micelli and Aiello 2019; Nobili and Signorini 2017). Presently, Italian and international guidelines consider this aspect to be relevant. As an example, the Italian guidelines (CSLP 2018) for the identification, qualification, and control of acceptance of FRCM systems to be used for the structural strengthening of existing constructions state that the mechanical performance of FRCM systems must be defined by considering specific environmental conditions, such as the presence of humidity, rainfall, freeze/thaw cycles, and exposure to saline and alkaline environments. The guidelines also prescribe assessing the behavior of these systems under thermal variations, through the execution of tensile tests on FRCM coupons at specific temperatures, corresponding to the upper limit of the temperature interval declared by the producer, within which the performances of the FRCM system should be guaranteed. A criterion was introduced for the

[1]Dept. of Civil, Chemical, Environmental and Materials Engineering, Univ. of Bologna, Viale Risorgimento 2, 40136 Bologna, Italy (corresponding author). ORCID: https://orcid.org/0000-0003-1484-3853. Email: francesca.ferretti10@unibo.it

[2]CIRI Buildings and Construction, Univ. of Bologna, Via del Lazzaretto 15/5, 40131 Bologna, Italy. Email: annarosa.tilocca@unibo.it

[3]CIRI Buildings and Construction, Univ. of Bologna, Via del Lazzaretto 15/5, 40131 Bologna, Italy. Email: a.incerti@unibo.it

[4]Dept. of Civil, Chemical, Environmental and Materials Engineering, Univ. of Bologna, Viale Risorgimento 2, 40136 Bologna, Italy. ORCID: https://orcid.org/0000-0002-5314-4687. Email: claudio.mazzotti@unibo.it

[5]Dept. of Civil, Chemical, Environmental and Materials Engineering, Univ. of Bologna, Viale Risorgimento 2, 40136 Bologna, Italy. Email: marco.savoia@unibo.it

Note. This manuscript was submitted on January 27, 2022; approved on May 9, 2022; published online on August 16, 2022. Discussion period open until January 16, 2023; separate discussions must be submitted for individual papers. This paper is part of the ***Journal of Composites for Construction***, © ASCE, ISSN 1090-0268.

qualification and control of acceptance of FRCM systems based on comparisons between the axial stress versus strain curves of thermally conditioned samples and those of the reference samples tested at ambient temperature: the differences between the curves, at each strain value, should be limited to ±15%.

Nevertheless, of the few studies that have looked into the behavior of FRCM samples subjected to thermal variation, high temperatures were prescribed to some FRCM systems, either with the objective of studying their tensile or bond behavior (Donnini et al. 2017; Iorfida et al. 2019; Maroudas and Papanicolaou 2017; Ombres et al. 2018). These works focused on the influence of thermal conditioning, using either an oven or a climatic chamber, on the behavior of fibers, mortar matrix, and the matrix-to-fiber interface. The latter result was strongly influenced by the presence of an organic coating applied to the fibers. However, these studies were more related to assessments of the fire resistance of these systems, given the very high temperatures prescribed, while the effect of lower temperatures, such as those that an FRCM system might experience when applied to an external surface of a building under service conditions (e.g., strong sunlight exposure), have been less frequently studied and should be further investigated.

The objective of the present research was to evaluate the effect of thermal variations on the tensile behavior of various FRCM systems. For this purpose, an experimental campaign was conducted, in which tensile tests were performed on unconditioned and thermally conditioned FRCM samples. The considered thermal variations were comparable to those that an FRCM system might be subjected to under service conditions. Several thermal scenarios were considered to investigate the effect of different target temperatures, exposure periods, test conditions, heating procedures, and heating sources on the tensile test results, and to identify the optimal conditioning and testing procedures. Ninety tensile tests were performed on six different FRCM systems, made of steel, basalt, or aramid-glass fibers coupled with lime- or cement-based mortar matrices.

Materials and Testing Methods

The FRCM strengthening systems investigated in the present experimental campaign were obtained by combining various mortar matrices with different types of reinforcing fibers (according to manufacturer recommendations). Three different premixed mortar matrices were adopted:

1. a cement-based mortar (hereafter CEM) and
2. two natural hydraulic lime-based mortars (NHL1 and NHL2).

The following types of reinforcing fibers were used:

1. S [Fig. 1(a)]: high-strength unidirectional stainless-steel fibers, with a weight density of 650 g/m^2, an effective cross section of the strands of 0.483 mm^2, and an equivalent thickness of 0.063 mm;
2. B1 [Fig. 1(b)]: balanced bidirectional basalt grid, with a total weight density of 210 g/m^2, a spacing of 16 mm, a yarn section of 0.544 mm^2, and an equivalent thickness of 0.034 mm in each direction;
3. B2 [Fig. 1(c)]: balanced bidirectional basalt grid, with a total weight density of 365 g/m^2, a spacing of 9 mm, a yarn section of 0.496 mm^2, and an equivalent thickness of 0.054 mm in each direction;
4. B3 [Fig. 1(d)]: balanced bidirectional basalt grid, with a total weight density of 200 g/m^2, a spacing of 17 mm, a yarn section of 0.544 mm^2, and an equivalent thickness of 0.032 mm in each direction; and
5. AG [Fig. 1(e)]: unbalanced bidirectional coated aramid-glass grid, with a total weight density of 250 g/m^2, spacings of 15 mm (warp direction, i.e., the direction along which the tensile tests were performed) and 18 mm (weft direction), and equivalent thicknesses of 0.031 and 0.049 mm, respectively, for the warp and weft directions; the section of the single yarns was equal to 0.465 and 0.875 mm^2 in the warp and weft directions, respectively.

The following combinations of the two materials were considered in investigating the influence of the mortar matrix and reinforcing fiber properties on the thermal behavior of the FRCM strengthening systems: S-CEM, S-NHL1, B1-NHL1, B2-NHL1, B3-NHL2, AG-NHL2. For each system, 15 FRCM coupons were prepared. The length and thickness of the coupons were 500 and 10 mm, respectively, while the width, as reported in the following, was a function of the number of bundles inside the specimens and of the bundle spacing (CSLP 2018). The coupons were cured in a laboratory-controlled environment (T = 22°C ± 1°C, RH = 60% ± 5%) for 28 days before being subjected to a specific thermal conditioning, which concluded with a direct tensile test.

Mechanical Characterization of the Materials

Mortar Matrix

The mechanical properties of the mortar matrices were determined through standard laboratory tests, in accordance with EN 1015-11 (EN 1015-11, CEN 2019). For each mortar matrix, three prismatic specimens, with dimensions 160 × 40 × 40 mm^3, were cast and cured in a laboratory-controlled environment for 28 days and then subjected to a three-point bending test at ambient temperature (22°C). Uniaxial compression tests were then performed on the specimens that resulted from the flexural tests. Cyclic compression tests, according to EN 12390-13 (EN 12390-13, CEN 2013), were also conducted on three standard prismatic specimens for each mortar typology, of dimensions 160 × 40 × 40 mm^3, to evaluate the elastic modulus.

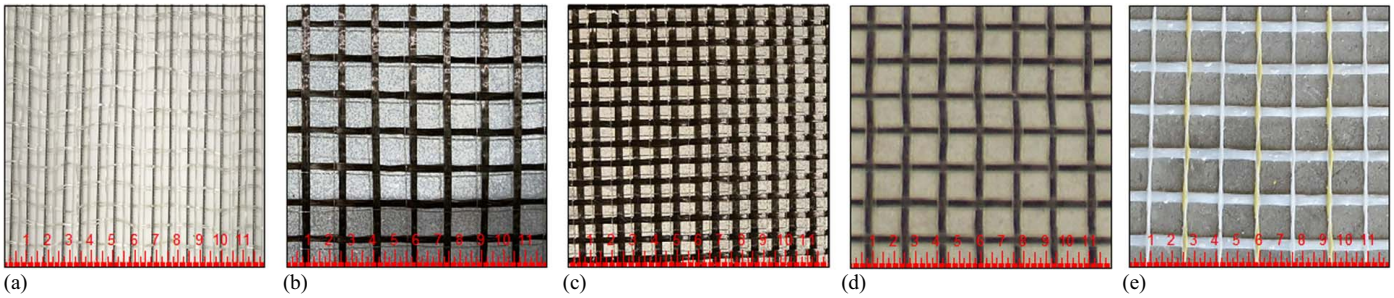

Fig. 1. Reinforcing fibers: (a) S; (b) B1; (c) B2; (d) B3; and (e) AG.

J. Compos. Constr., 2022, 26(5): 04022067

To investigate the effect of temperature on the mortar matrix flexural strength, three-point bending tests were also performed on three specimens for each mortar matrix at different temperatures: 50°C and 80°C. The specimens were positioned inside a thermal chamber (to be described). The temperature was increased at a rate of 30°C/h and the test started after attainment of the target temperature. The experimental results, in terms of mortar matrix compressive strength, $f_{m,c}$, and flexural strength, $f_{m,fl}$, at the reference condition (22°C) and at different temperatures, are reported in Table 1, together with the values of the elastic modulus, E_m, evaluated at ambient temperature only. Natural hydraulic lime-based mortars (hereafter NHL1 and NHL2) are characterized by a progressive reduction in flexural strength as the temperature increases; this effect is less evident in cementitious mortar (CEM).

Dry Fibers

The mechanical characterization of the dry fibers adopted in the present experimental campaign was carried out following the Italian guidelines (CSLP 2018) and in line with International Standards (ACI 549.6R-20, ACI 2020). Tensile tests were performed on bidirectional grid- or unidirectional strip samples, nine for each reinforcing fiber typology. The length of the specimens was 500 mm and the width ranged between 60 and 64 mm. A different number of bundles was tested, according to the bundle spacing of the reinforcing grids or strips: four bundles were tested for B1, B3, and AG1, seven bundles for B2, and eight bundles for S1. Fiber-reinforced polymer (FRP) tabs were applied with epoxy resin to both ends of the specimens to transfer the load and prevent premature ruptures.

Tests were conducted under displacement control using a servo-hydraulic machine with a maximum capacity of 100 kN and prescribing a displacement rate equal to 0.5 mm/min. The deformations in the center of the coupons were measured by means of an extensometer with a gauge length of 200 mm.

The results of the direct tensile tests are reported in Table 1 in terms of average tensile strength, σ_u, average ultimate strain, ε_u, and average dry fiber elastic modulus, E_f (coefficients of variation [CoVs] are reported in parenthesis). Even though both fiber and matrices codes are specified for the various FRCM systems, "dry fibers" and "mortar matrix" of course indicate the properties of the two materials alone.

Direct Tensile Test Setup

The direct tensile tests were performed on FRCM coupons using a servo-hydraulic testing machine with a maximum load capacity of 100 kN and equipped with an onboard class 0.5 load cell (Fig. 2). The extremities of the specimens were strengthened with FRP composite tabs, similar to the ones described for tests on the dry fibers, to avoid local failures due to grip clamping. The tests were performed under displacement control, with a rate of 0.2 mm/min in the first part of the test, until the end of the cracking phase, which was then increased to 0.5 mm/min in the last part of the test (CSLP 2018). The strain was measured by means of an extensometer, positioned in the central part of the samples, with a gauge length of 200 mm. It is worth mentioning that the FRCM coupons were characterized by the same number of bundles as the dry fiber samples.

In the present experimental campaign, most of the direct tensile tests were performed with the sample inside a thermal chamber, as shown in Fig. 2(*a*). The chamber is airtight, with fiberglass insulation between the outer liner and the stainless-steel inner liner. It is equipped with a multipaned, tempered glass window. The working temperature range is $-129°C \div +315°C$, with a maximum heating rate of 550°C/h. The thermal chamber and the servo-hydraulic machine were perfectly locked together to ensure a controlled heating environment during the tests.

Testing Procedures

The direct tensile tests were performed at ambient temperature (22°C) and under several thermal conditioning protocols that considered different target temperatures, exposure periods, test conditions, procedures, and adopted heating sources. Three different target temperatures were selected: 40°C, 50°C, and 80°C. The highest target temperature (80°C) was chosen according to Italian building code recommendations (Ministero delle Infrastrutture e dei Trasporti 2018) concerning the strongest effects of solar radiation on the maximum temperature of external building surfaces. The FRCM samples were exposed to the target temperature for different periods of time prior to test: 5 min (short-term exposure) or 360 min (long-term exposure).

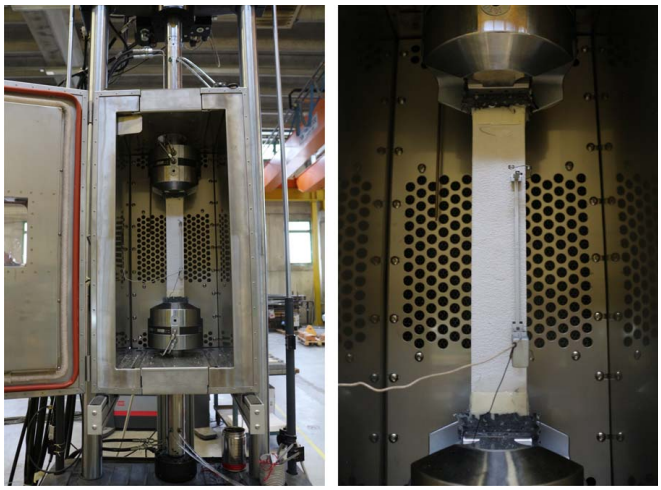

(a) (b)

Fig. 2. Setup of the direct tensile test: (a) climatic chamber; and (b) zoom on the FRCM coupon.

Table 1. FRCM strengthening systems: mechanical properties of the materials (CoV in parenthesis)

		Dry fibers			Mortar matrix				
Designation	FRCM system	σ_u (MPa)	ε_u (%)	E_f (GPa)	E_m (GPa)	$f_{m,c}$ (MPa)	$f_{m,fl}$ (MPa)	$f_{m,fl(50\,°C)}$ (MPa)	$f_{m,fl(80\,°C)}$ (MPa)
S1	S-CEM	2,221 (2.3)	1.38 (6.3)	229 (3.2)	23 (4.7)	49.8 (6.7)	7.2 (10.3)	4.9 (8.1)	5.5 (12.4)
S2	S-NHL1	2,221 (2.3)	1.38 (6.3)	229 (3.2)	10 (10.2)	20.4 (3.7)	8.1 (9.5)	6.4 (11.9)	4.0 (8.6)
S3	B1-NHL1	1,201 (3.1)	1.97 (3.1)	78 (3.5)	10 (10.2)	20.4 (3.7)	8.1 (9.5)	6.4 (11.9)	4.0 (8.6)
S4	B2-NHL1	1,368 (4.5)	2.01 (7.8)	82 (1.8)	10 (10.2)	20.4 (3.7)	8.1 (9.5)	6.4 (11.9)	4.0 (8.6)
S5	B3-NHL2	1,160 (3.3)	2.20 (5.1)	76 (6.8)	12 (0.3)	11.6 (10.9)	3.1 (8.7)	2.8 (16.5)	2.5 (13.2)
S6	AG-NHL2	1,467 (11.4)	1.20 (8.4)	115 (9.3)	12 (0.3)	11.6 (10.9)	3.1 (8.7)	2.8 (16.5)	2.5 (13.2)

Table 2. Conditioning protocols and testing procedures

Code	Preheating source	Temperature (°C)	Exposure time (min)	Test condition
Reference	—	22	—	—
C40-5_TC	Thermal Chamber	40	5	Inside the thermal chamber
C50-5_TC	Thermal Chamber	50	5	Inside the thermal chamber
C80-5_TC	Thermal Chamber	80	5	Inside the thermal chamber
C80-360_TC	Thermal Chamber	80	360	Inside the thermal chamber
O80-360_TC	Oven	80	360	Inside the thermal chamber
O80-360_NTC	Oven	80	360	Outside the thermal chamber

In order to test different conditioning protocols, the adopted heating source prior to mechanical test was either a thermal chamber or an oven, while the mechanical tests were conducted inside or outside the thermal chamber.

For each FRCM system, the direct tensile tests were conducted at ambient temperature (22°C) on three reference samples, while two direct tensile tests were performed according to each of the following conditioning protocols and testing procedures (Table 2):

1. Procedure CXX-5_TC (where XX = 40, 50, 80 indicates the target temperature), with both preliminary short-term exposure and test inside the thermal chamber: (1) the FRCM coupon was heated up with a thermal gradient of 30°C/h; (2) the target temperature (40°C, 50°C, or 80°C) was maintained for 5 min; (3) the tensile test was performed.
2. Procedure C80-360_TC, with both long-term exposure and testing inside the thermal chamber: (1) the FRCM coupon was heated up to 80°C with a thermal gradient of 30°C/h; (2) the target temperature was maintained for 360 min; (3) the tensile test was performed. This thermal conditioning is the one prescribed by the Italian guidelines (CSLP 2018).
3. Procedure O80-360_TC, with long-term exposure in the oven and testing inside the thermal chamber: (1) the FRCM coupon was positioned in the oven and heated up to 80°C; (2) the target temperature was maintained for 360 min; (3) the sample was removed from the oven and positioned inside the thermal chamber (required time approximately 10 min), where the temperature was already set to 80°C; and (d) the tensile test was performed.
4. Procedure O80-360_NTC, with long-term exposure in the oven and test at ambient temperature: (1) the FRCM coupon was positioned in the oven and heated up to 80°C; (2) the target temperature was maintained for 360 min; (3) the sample was removed from the oven; and (4) the tensile test was performed at ambient temperature immediately after. In this case, the temperature of the specimen during the test was not controlled.

Temperature profiles corresponding to the described thermal conditioning protocols are reported in Fig. 3.

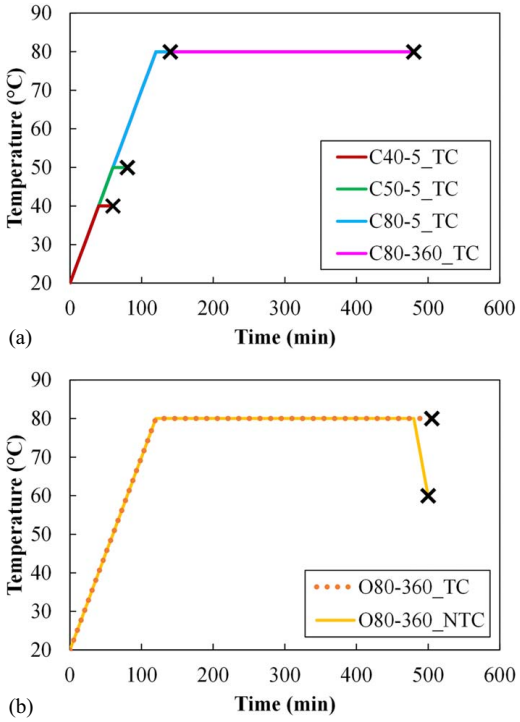

Fig. 3. Temperature profiles for thermal conditioning with different heating sources: (a) thermal chamber; and (b) oven.

Experimental Results and Discussion

For each FRCM system and thermal conditioning, a representative normal stress versus strain curve was selected from all the results and is shown in Figs. 4–9. Normal stress was calculated by dividing the force by the dry fibers' cross-section area only. In all cases, typical trilinear behavior was observed (Fig. 10), characterized by an initial uncracked phase, a cracking phase, and a fully cracked phase; in the latter stage, the role of the fiber was prevalent. The various drops in stress in the figures indicate the formation of transverse cracks in the matrix (tests were performed under displacement control).

A preliminary analysis of the results showed that thermal conditioning may have affected the behavior of the specimens. Typically, stresses at first cracking were lower for tests conducted after heating, with respect to those performed at ambient temperature, and those with heating and testing at 80°C usually exhibited the lowest stress. This result was correlated with a reduction in the tensile strength of the mortar matrix, documented through the flexural tests (Table 1). Tests conducted outside the thermal chamber after heating showed stresses at first cracking that are were usually intermediate: between those of the tests conducted at ambient temperature and those at 80°C. A more detailed analysis of the results requires comparison of data at significant points of the curves, which follows.

The results of the 90 tests performed on the different FRCM systems are given in Tables 3 and 4, where the stresses, σ_i, and strains, ε_i, of three representative points are reported. These points were identified as corresponding to the end of the different phases in the trilinear behavior of the normal stress versus strain curves, as shown in Fig. 10. In particular, they corresponded to the formation of the first crack (i.e., first peak along the normal stress versus strain curve), to the end of the cracking phase, beyond which no further cracks formed, and to the failure point (i.e., ultimate stress and strain values), respectively. In more detail, the stress at the end of the cracking phase (σ_2) was identified as the stress value corresponding to the last peak of the cracking phase, which was defined as that characterized by a postpeak stress drop greater than 2% of the maximum stress. For Systems S1 and S2, the peaks within

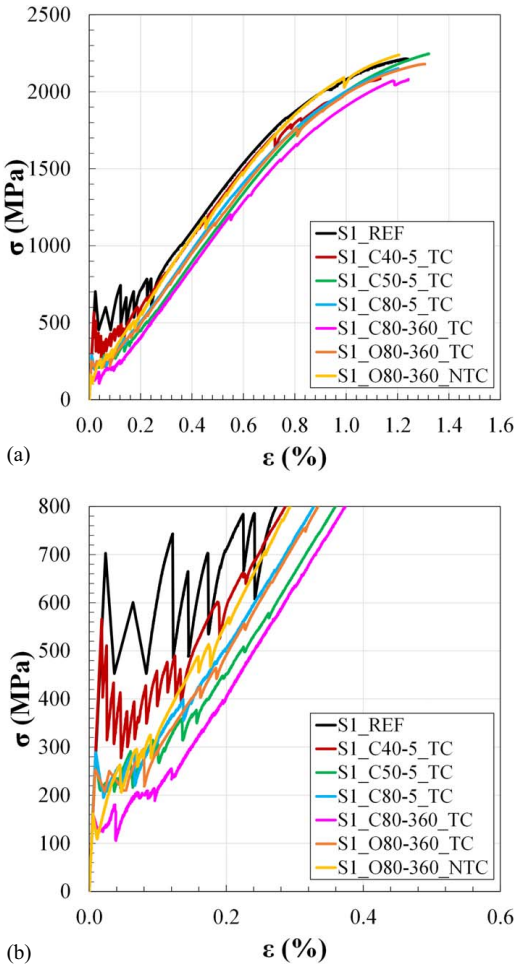

Fig. 4. Tensile test results for System S1 (S-CEM) subjected to different thermal conditioning procedures: (a) normal stress versus strain curves; and (b) zoom of the initial portion of the curves.

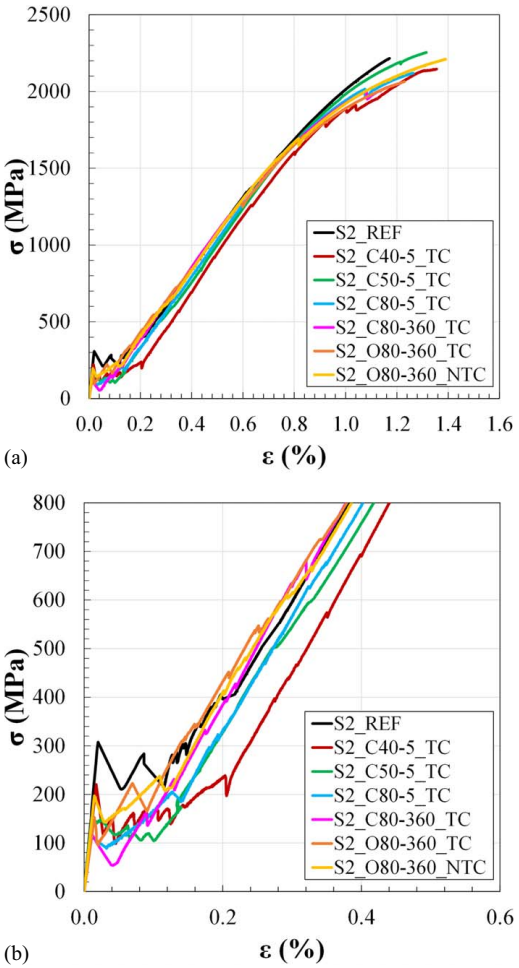

Fig. 5. Tensile test results for System S2 (S-NHL1) subjected to different thermal conditioning procedures: (a) normal stress versus strain curves; and (b) zoom of the initial portion of the curves.

the last branch of the curves, in which the behavior is no longer linear, were discarded. The elastic modulus, E_3, ideally representing the tangent to the initial portion of the third branch of the curves, was calculated as the secant modulus between the values of σ_2 and $1.2\sigma_2$.

In addition to the expected differences in stresses and strains during the tests among the tested FRCM systems, due to differences in the fiber or grid geometrical and mechanical properties and in the mortar matrix tensile strength, different cracking patterns were observed, as shown in Fig. 11 for tensile tests performed at ambient temperature. The failure mode of the coupons was always characterized by a tensile rupture of the fibers after the appearance of cracks within the matrix. The cracking pattern at failure was affected, as expected (Carozzi et al. 2017; Leone et al. 2017; Lignola et al. 2017; De Santis et al. 2017), by the different arrangements and axial stiffness of the fibers, since the development only a few or multiple cracks was related to the ability of the fibers to redistribute the stresses along the entire length of the FRCM coupons. This was particularly evident when comparing the failure mode of the FRCM systems with unidirectional steel fibers [Figs. 11(*a* and *b*)] with that of FRCM systems with bidirectional basalt or aramid-glass grids [Figs. 11(*c* and *d*)]: multiple cracks occurred in the former, while only a few cracks developed in the latter. If one FRCM system at a time is considered, it is worth noting that the same cracking patterns were observed at ambient temperature and at increased temperature, as can be seen by comparing the images in Figs. 11 and 12. In some cases, such as for Systems S1 and S2, a smoother stress versus strain behavior was observed during the cracking phase of the coupons at elevated temperature, with respect to the behavior at ambient temperature, characterized by fewer evident peaks and discontinuities. This corresponded to the formation of the same number of cracks in both cases, the temperature not influencing the cracking pattern.

As previously underlined, the normal stress versus strain curves (Figs. 4–9) showed that the behavior of the FRCM coupons was affected by thermal conditioning, especially in the first part of the test during the uncracked and cracking phases. Differences between the conditioned and the reference tests (22°C) can be observed in most cases in terms of stress at the first peak and an extension of the cracking phase. In the fully cracked phase, however, the behavior of the conditioned samples was similar to that observed in the FRCM samples tested at ambient temperature.

Effect of Thermal Conditioning

Comparisons between the effects of different thermal conditioning procedures for the various FRCM systems were carried out for different target temperatures, exposure periods, adopted heating sources (i.e., thermal chamber or oven), and test conditions (i.e., inside or outside the thermal chamber). In general, it can be observed from the data in Tables 3 and 4 that the values of σ_3 and E_3 were

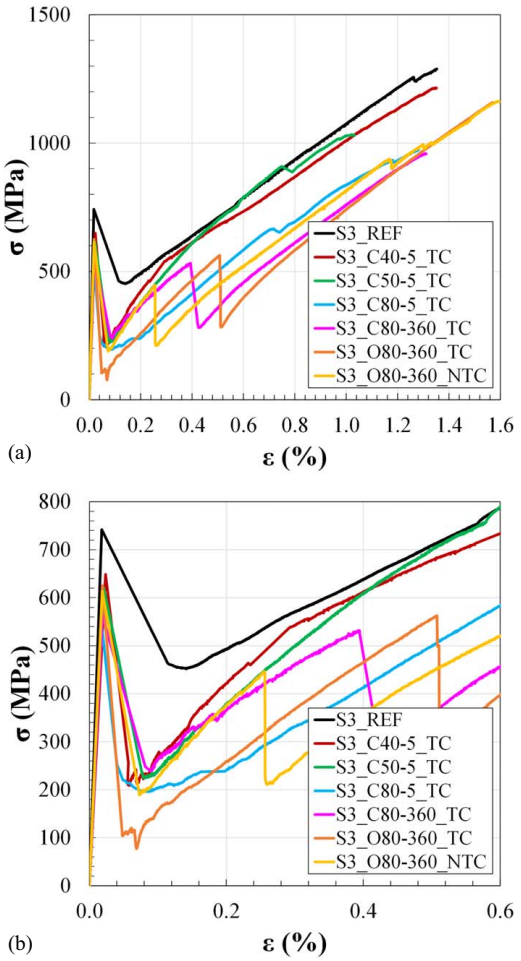

Fig. 6. Tensile test results for System S3 (B1-NHL1) subjected to different thermal conditioning procedures: (a) normal stress versus strain curves; and (b) zoom of the initial portion of the curves.

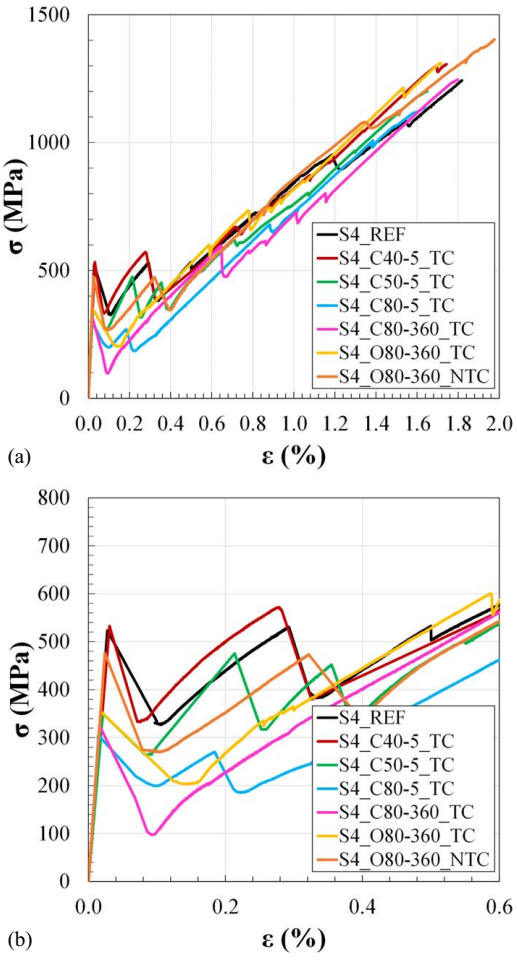

Fig. 7. Tensile test results for System S4 (B2-NHL1) subjected to different thermal conditioning procedures: (a) normal stress versus strain curves; (b) zoom of the initial portion of the curves.

closer to the reference results with respect to those of σ_1 and σ_2. They were also in good agreement with the results obtained on the dry fibers (Table 1).

The σ_1 values, corresponding to the first crack formation, seemed to be most affected by thermal conditioning. Significant average percentage variations were observed for the results on the conditioned samples (Tables 3 and 4), with values of σ_1 being significantly lower than the reference results in most cases. Concerning the effect of the different target temperatures in short-term exposure tests (C40-5_TC, C50-5_TC, C80-5_TC), it was noted that, with increasing temperature, the values of σ_1 were progressively lower than those of the unconditioned samples for the majority of the FRCM systems. These results confirmed what was previously observed in comparisons between normal stress versus strain curves in the cracking phase and will be further analyzed.

The results of the long-term (360 min) and short-term (5 min) exposure tests performed inside the thermal chamber at 80°C (C80-5_TC and C80-360_TC) were quite similar, especially for Systems S1, S2, S4, and S5. Only for S6 did the long-term exposure tests lead to values of σ_1 that were higher than the reference. Hence, based on the outcomes for the majority of the FRCM systems, it can be stated that the exposure period did not appreciably influence the results. However, it had a great impact on the total duration of the test and could be significantly reduced with respect to the 360 min recommended by the Italian guidelines (CSLP 2018) and adopted here for the long-term exposure tests, provided that a low thermal gradient is adopted.

Different conclusions can be drawn from the tests conducted with heating in the oven. The peculiarity of the thermal conditioning procedures involving use of the oven to heat the FRCM samples was that, after the temperature was held constant for 360 min, the coupons were removed from the oven and positioned inside or outside the thermal chamber to perform the tensile test. During this operation, the FRCM samples inevitably cooled down significantly due to the thinness of the coupons. Moreover, samples removed from the oven and tested inside the thermal chamber (O80-360_TC) did not immediately regain the target temperature, even if the thermal chamber was already set to 80°C; thus, the coupons were at a lower temperature when the tensile test started. The problem of temperature control was even more significant for tests performed outside the thermal chamber (O80-360_NTC): the coupon temperature decreased rapidly (see images in Fig. 13, taken with an infrared thermal imaging camera), reaching approximately 62°C at the beginning of the test starting 10 min after coupon removal from the oven, and 42°C at the appearance of the first mortar matrix cracking. At the end of the test, the temperature was approximately 29°C, confirming that tests must be conducted inside a thermal chamber in order to obtain reliable results. In several cases, the stress values at first cracking (σ_1) for specimens subjected to the thermal conditioning protocols with the use of the oven (O80-360_TC and O80-360_NTC) were

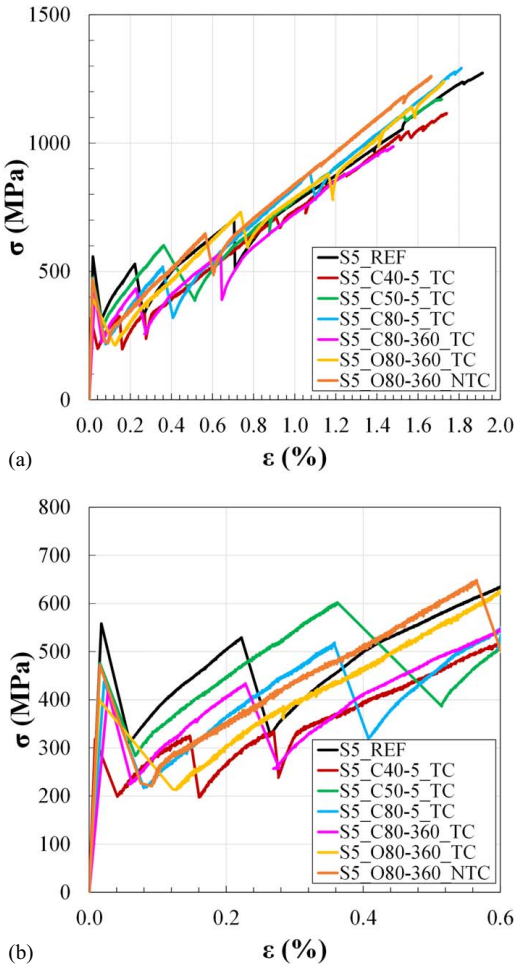

Fig. 8. Tensile test results for System S5 (B3_NHL2) subjected to different thermal conditioning procedures: (a) normal stress versus strain curves; (b) zoom of the initial portion of the curves.

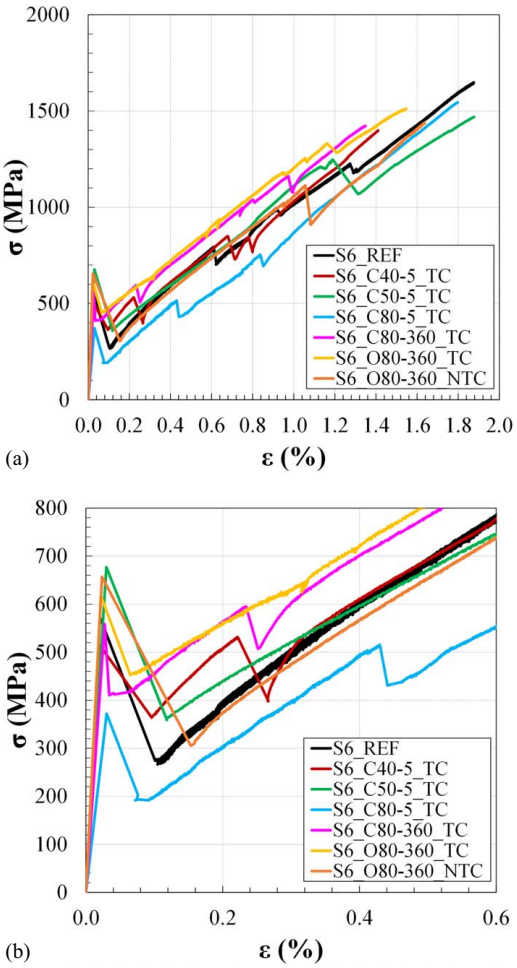

Fig. 9. Tensile test results for System S6 (AG-NHL2) subjected to different thermal conditioning procedures: (a) normal stress versus strain curves; (b) zoom of the initial portion of the curves.

greater than those obtained after long-term thermal exposure and testing inside the thermal chamber (C80-360_TC), supporting the conclusion that temperature had a significant effect on the tensile behavior of FRCM samples in the cracking phase: a decrease in temperature, due to the removal of the FRCM coupons from the oven, led to an increase in stress at first cracking (σ_1). To reduce the uncertainties related to the actual temperature of the samples and, consequently, to ensure correct detection of the thermal effects on FRCM, the tests should be conducted in the thermal chamber for their entire duration, that is, both for the heating and the testing phases.

Effect of Temperature Variations on the Stress at First Cracking

From the obtained results, it can be stated that an increase in temperature up to 80°C did not significantly affect the mechanical performances of the fibers, although it could determine a variation in the mortar matrix tensile strength, as also evidenced by the flexural tests performed on the mortar matrix (Table 1). The fiber-to-matrix interaction was also modified by the temperature, due either to the coating applied to the fibers or to the presence of organic components within the mortar mix, whose stiffness was reduced when the temperature rose. Even though the percentage of organic content, in weight, was lower than the 10% inorganic binder content,

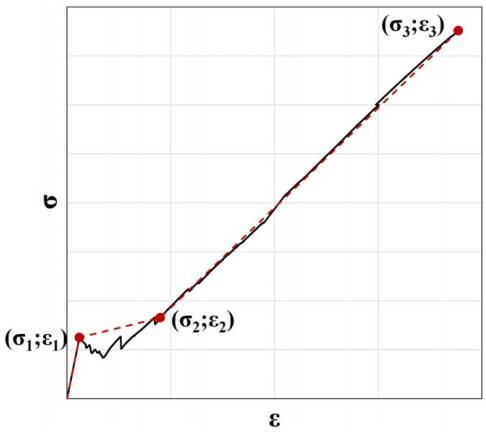

Fig. 10. Typical trilinear behavior of an FRCM system subjected to direct tensile tests.

the performance of these materials could have been significantly affected by temperature.

To better analyze the effect of the temperature increase on the cracking phase, the tensile stress in the mortar matrix at first cracking (σ_{mx}) was evaluated for all the tests as the force registered at first peak divided by the cross section of the FRCM coupons,

Table 3. Results of direct tensile tests on the FRCM systems S1 (S-CEM), S2 (S-NHL1) and S3 (B1-NHL1)

Sample	Width (mm)	σ_1 (MPa)	$\frac{\sigma_{1,i}}{\sigma_{1,REF}} \cdot 100$ (%)	ε_1 (%)	σ_2 (MPa)	ε_2 (%)	σ_3 (MPa)	ε_3 (%)	E_3 (GPa)
S1_REF_1	60	573	—	0.019	604	0.222	2,211	1.189	219
S1_REF_2	—	501	—	0.016	729	0.277	2,171	1.171	199
S1_REF_3	—	703	—	0.024	786	0.269	2,215	1.243	221
S1_C40-5_TC_1	—	566	87	0.018	602	0.202	2085	1.133	227
S1_C40-5_TC_2	—	464	—	0.014	780	0.243	2,100	1.089	208
S1_C50-5_TC_1	—	280	53	0.009	359	0.147	2,247	1.322	223
S1_C50-5_TC_2	—	349	—	0.011	409	0.156	2,280	1.308	229
S1_C80-5_TC_1	—	155	38	0.005	585	0.278	2009	1.130	216
S1_C80-5_TC_2	—	289	—	0.010	399	0.150	2,152	1.202	228
S1_C80-360_TC_1	—	151	26	0.005	323	0.156	2053	1.262	218
S1_C80-360_TC_2	—	155	—	0.005	260	0.133	2081	1.242	227
S1_O80-360_TC_1	—	253	42	0.009	296	0.101	2,180	1.307	216
S1_O80-360_TC_2	—	244	—	0.008	394	0.152	1955	1.129	203
S1_O80-360_NTC_1	—	162	27	0.006	308	0.093	2,201	1.198	232
S1_O80-360_NTC_2	—	161	—	0.006	514	0.186	2,240	1.206	214
S2_REF_1	60	250	—	0.024	253	0.127	2,187	1.317	205
S2_REF_2	—	250	—	0.025	250	0.106	2,101	1.132	206
S2_REF_3	—	308	—	0.020	267	0.124	2,216	1.171	205
S2_C40-5_TC_1	—	220	76	0.017	239	0.214	2,146	1.355	229
S2_C40-5_TC_2	—	191	—	0.013	209	0.122	2,226	1.476	226
S2_C50-5_TC_1	—	153	69	0.011	153	0.128	2,255	1.307	236
S2_C50-5_TC_2	—	219	—	0.022	282	0.149	2075	1.216	205
S2_C80-5_TC_1	—	111	46	0.011	205	0.148	2,119	1.264	234
S2_C80-5_TC_2	—	134	—	0.009	367	0.205	2,170	1.345	233
S2_C80-360_TC_1	—	109	43	0.010	160	0.089	2,164	1.410	225
S2_C80-360_TC_2	—	121	—	0.010	121	0.072	2051	1.209	224
S2_O80-360_TC_1	—	153	66	0.015	223	0.109	2064	1.230	225
S2_O80-360_TC_2	—	202	—	0.016	209	0.112	2,131	1.449	237
S2_O80-360_NTC_1	—	199	74	0.015	199	0.088	2,302	1.419	226
S2_O80-360_NTC_2	—	197	—	0.015	238	0.135	2,210	1.390	212
S3_REF_1	64	678	—	0.019	678	0.508	1,257	1.312	84
S3_REF_2	—	735	—	0.020	735	0.535	1,196	1.191	81
S3_REF_3	—	742	—	0.018	742	0.549	1,289	1.353	71
S3_C40-5_TC_1	—	649	80	0.024	649	0.455	1,215	1.351	66
S3_C40-5_TC_2	—	494	—	0.016	494	0.346	1,219	1.360	72
S3_C50-5_TC_1	—	442	74	0.014	442	0.182	1,137	1.242	71
S3_C50-5_TC_2	—	621	—	0.021	621	0.413	1,033	1.032	86
S3_C80-5_TC_1	—	553	71	0.017	553	0.563	973	1.281	83
S3_C80-5_TC_2	—	464	—	0.015	464	0.358	1,157	1.326	82
S3_C80-360_TC_1	—	713	89	0.023	829	1.065	1,049	1.380	76
S3_C80-360_TC_2	—	563	—	0.019	531	0.694	959	1.311	78
S3_O80-360_TC_1	—	625	89	0.019	563	0.778	1,159	1.571	74
S3_O80-360_TC_2	—	654	—	0.022	540	0.591	996	1.301	67
S3_O80-360_NTC_1	—	613	88	0.019	446	0.500	1,163	1.596	74
S3_O80-360_NTC_2	—	650	—	0.020	769	0.938	989	1.311	70

Table 4. Results of direct tensile tests on the FRCM systems S4 (B2-NHL1), S5 (B3-NHL2), and S6 (AG-NHL2)

Sample	Width (mm)	σ_1 (MPa)	$\frac{\sigma_{1,i}}{\sigma_{1,REF}} \cdot 100$ (%)	ε_1 (%)	σ_2 (MPa)	ε_2 (%)	σ_3 (MPa)	ε_3 (%)	E_3 (GPa)
S4_REF_1	64	523	—	0.028	952	1.323	1,243	1.818	68
S4_REF_2	—	506	—	0.026	925	1.263	1,286	1.949	67
S4_REF_3	—	480	—	0.032	430	0.363	1,434	1.977	62
S4_C40-5_TC_1	—	533	95	0.031	670	0.769	1,306	1.744	76
S4_C40-5_TC_2	—	419	—	0.023	419	0.306	1,368	1.823	70
S4_C50-5_TC_1	—	350	68	0.021	452	0.489	1,201	1.649	74
S4_C50-5_TC_2	—	330	—	0.018	971	1.345	1,151	1.606	78
S4_C80-5_TC_1	—	305	66	0.015	270	0.352	1,136	1.638	73
S4_C80-5_TC_2	—	359	—	0.021	359	0.400	1,157	1.515	74
S4_C80-360_TC_1	—	420	74	0.019	727	1.059	1,176	1.780	75
S4_C80-360_TC_2	—	326	—	0.016	746	1.113	1,246	1.798	75
S4_O80-360_TC_1	—	464	81	0.024	951	1.237	1,140	1.515	76
S4_O80-360_TC_2	—	355	—	0.018	734	0.862	1,311	1.716	77
S4_O80-360_NTC_1	—	478	95	0.025	1,059	1.286	1,318	1.708	76
S4_O80-360_NTC_2	—	476	—	0.024	474	0.514	1,403	1.977	77

Table 4. (*Continued*.)

Sample	Width (mm)	σ_1 (MPa)	$\frac{\sigma_{1,i}}{\sigma_{1,REF}} \cdot 100$ (%)	ε_1 (%)	σ_2 (MPa)	ε_2 (%)	σ_3 (MPa)	ε_3 (%)	E_3 (GPa)
S5_REF_1	68	558	—	0.018	702	0.886	1,273	1.914	55
S5_REF_2	—	542	—	0.015	1,019	1.433	1,132	1.606	56
S5_REF_3	—	521	—	0.017	509	0.452	1,161	1.609	56
S5_C40-5_TC_1	—	318	57	0.009	711	0.958	1,116	1.739	57
S5_C40-5_TC_2	—	296	—	0.008	508	0.571	1,194	1.791	62
S5_C50-5_TC_1	—	476	94	0.016	602	0.709	1,171	1.716	61
S5_C50-5_TC_2	—	534	—	0.018	547	0.793	1,111	1.835	59
S5_C80-5_TC_1	—	438	85	0.015	887	1.174	1,292	1.811	64
S5_C80-5_TC_2	—	485	—	0.017	488	0.626	1,197	1.726	63
S5_C80-360_TC_1	—	486	84	0.005	613	0.720	976	1.382	65
S5_C80-360_TC_2	—	418	—	0.027	569	0.766	987	1.480	60
S5_O80-360_TC_1	—	402	65	0.015	880	1.211	1,241	1.725	61
S5_O80-360_TC_2	—	303	—	0.010	729	1.043	1,068	1.662	63
S5_O80-360_NTC_1	—	394	80	0.013	979	1.242	1,295	1.780	61
S5_O80-360_NTC_2	—	472	—	0.015	648	0.719	1,261	1.664	65
S6_REF_1	64	573	—	0.020	1,227	1.349	1,648	1.876	82
S6_REF_2	—	456	—	0.015	849	0.870	1,806	2.006	83
S6_REF_3	—	617	—	0.023	915	0.974	1,721	2.006	82
S6_C40-5_TC_1	—	419	85	0.030	695	0.786	1,428	1.824	81
S6_C40-5_TC_2	—	515	—	0.020	847	0.824	1,399	1.377	88
S6_C50-5_TC_1	—	677	105	0.030	1,247	1.534	1,469	1.878	85
S6_C50-5_TC_2	—	475	—	0.017	1,142	1.279	1,578	1.832	84
S6_C80-5_TC_1	—	562	85	0.035	812	1.053	1,756	2.086	85
S6_C80-5_TC_2	—	372	—	0.030	755	0.894	1,545	1.797	83
S6_C80-360_TC_1	—	558	111	0.027	1,162	1.037	1,422	1.348	82
S6_C80-360_TC_2	—	659	—	0.034	1,205	0.830	1,680	1.431	83
S6_O80-360_TC_1	—	513	103	0.019	1,381	1.437	1,608	1.753	87
S6_O80-360_TC_2	—	618	—	0.022	1,332	1.272	1,513	1.547	84
S6_O80-360_NTC_1	—	657	96	0.023	1,113	1.270	1,440	1.636	82
S6_O80-360_NTC_2	—	397	—	0.019	907	0.874	1,828	1.991	85

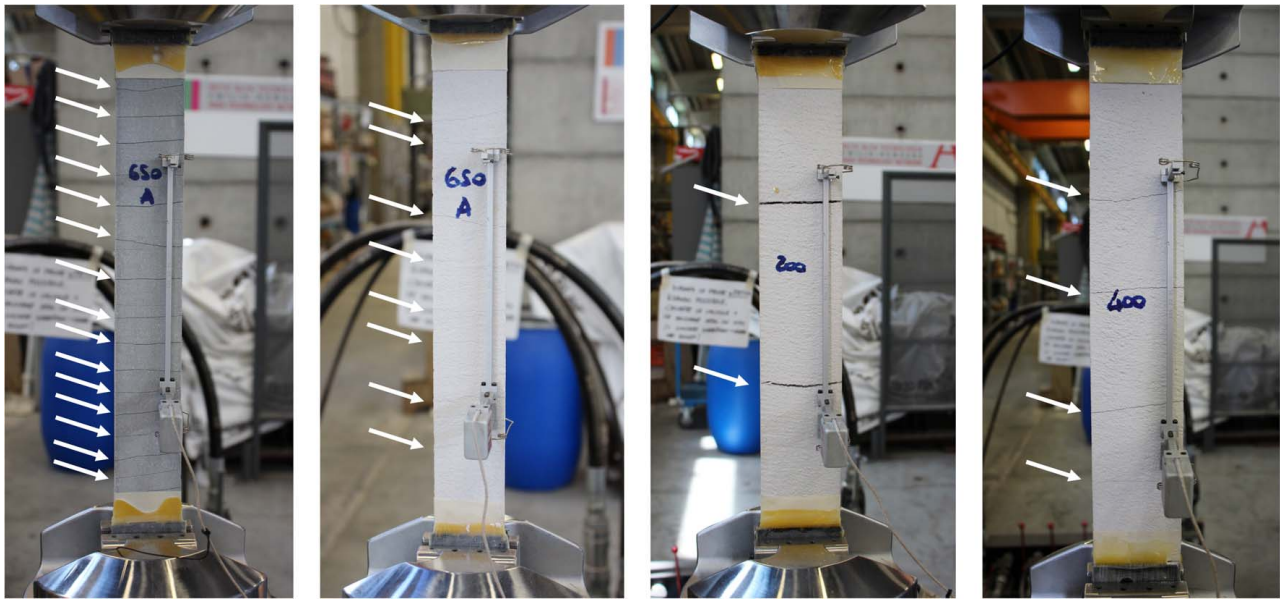

(a) (b) (c) (d)

Fig. 11. Representative failure modes for tests at ambient temperature: (a) S1 (S-CEM); (b) S2 (S-NHL1); (c) S3 (B1-NHL1); and (d) S4 (B2-NHL1). Arrows indicate the transverse cracks.

homogenized with respect to the mortar matrix. This stress was plotted against temperature, as shown in Fig. 14, considering only the results from tests performed inside the thermal chamber, given the uncertainties about the temperature of the FRCM coupons during the other tests. Clear trends were observed for FRCM System S1, where the CEM matrix was adopted, and S2 and S4, with the NHL1 matrix [Figs. 14(*a*, *b*, and *d*) respectively], with values of σ_{mx} strongly decreasing as the temperature increased. For Systems S5 and S6, realized with the mortar NHL2, a clear tensile stress trend in the mortar matrix at first cracking

J. Compos. Constr., 2022, 26(5): 04022067

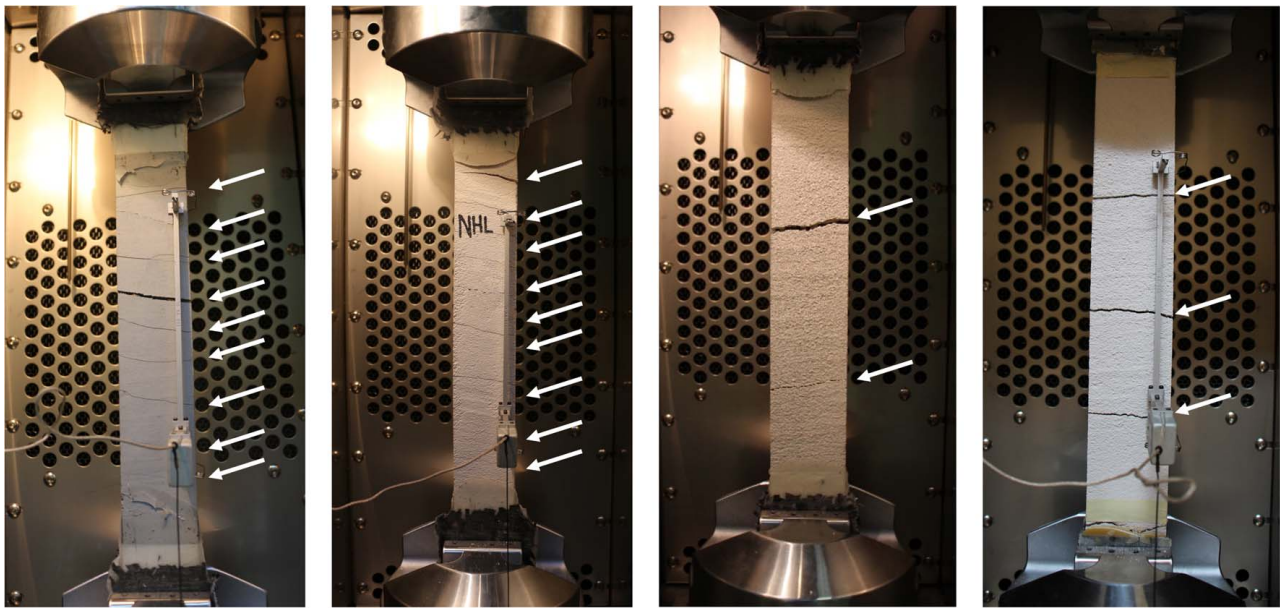

Fig. 12. Representative failure modes for tests after heating inside the thermal chamber: (a) S1 (S-CEM); (b) S2 (S-NHL1); (c) S3 (B1-NHL1); and (d) S4 (B2-NHL1). Arrows indicate the transverse cracks.

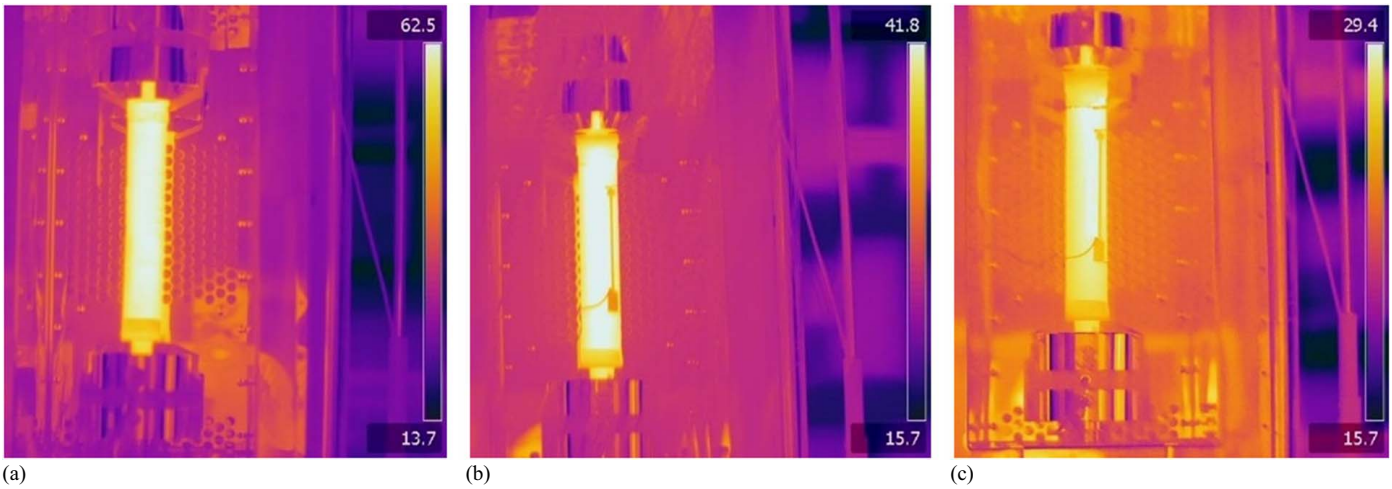

Fig. 13. Thermal images of an FRCM coupon subjected to long-term exposure in the oven and tested at ambient temperature: (a) beginning of the test; (b) first mortar matrix cracking; and (c) end of the test.

was not recognizable and correlation with the temperature could not be established.

Effect of Fiber and Grid Properties on the Stress at First Cracking

Fig. 15 shows a comparison between the performances of different mortar matrices with the objective of analyzing the effects of the fiber or grid properties on the stress at first cracking. Only tests conducted in the thermal chamber for FRCM systems with mortar matrices NHL1 and NHL2 were considered here because they allowed comparisons to be adopted in more than one FRCM system. The average value of the stress in the mortar matrix at first cracking, σ_{mx}, was evaluated for the different target temperatures. As far as the mortar matrix NHL1 [Fig. 15(*a*)] is concerned, similar results, in terms of σ_{mx}, were obtained for Systems S3 and S4 at the same temperature. Slight differences may be due to small variations in terms of weight density, bundle spacing, and axial stiffness. At the target temperature of 40°C, a higher dispersion on the results at first peak was registered. Significantly lower values of σ_{mx} were instead observed for System S2 for all the target temperatures, highlighting the fact that the stress at first cracking depended not only on the mortar matrix properties, but also on the fiber or grid characteristics. These differences can be explained by (1) the intrinsic dissimilarities between the systems, that is, unidirectional fibers (S2) or bidirectional grids (S3 and S4), the latter also characterized by the presence of transversal bundles; and (2) the differences in terms of the axial stiffness of those fibers, which could influence the development of the cracking process.

The results for stress in the mortar matrix at first cracking σ_{mx} for Systems S5 and S6 [Fig. 15(*b*)], in which the mortar matrix NHL2 was adopted, were in general quite similar. Small differences can be related to variations in the grid properties of the two systems, as discussed for the mortar matrix NHL1 (Systems S3 and S4).

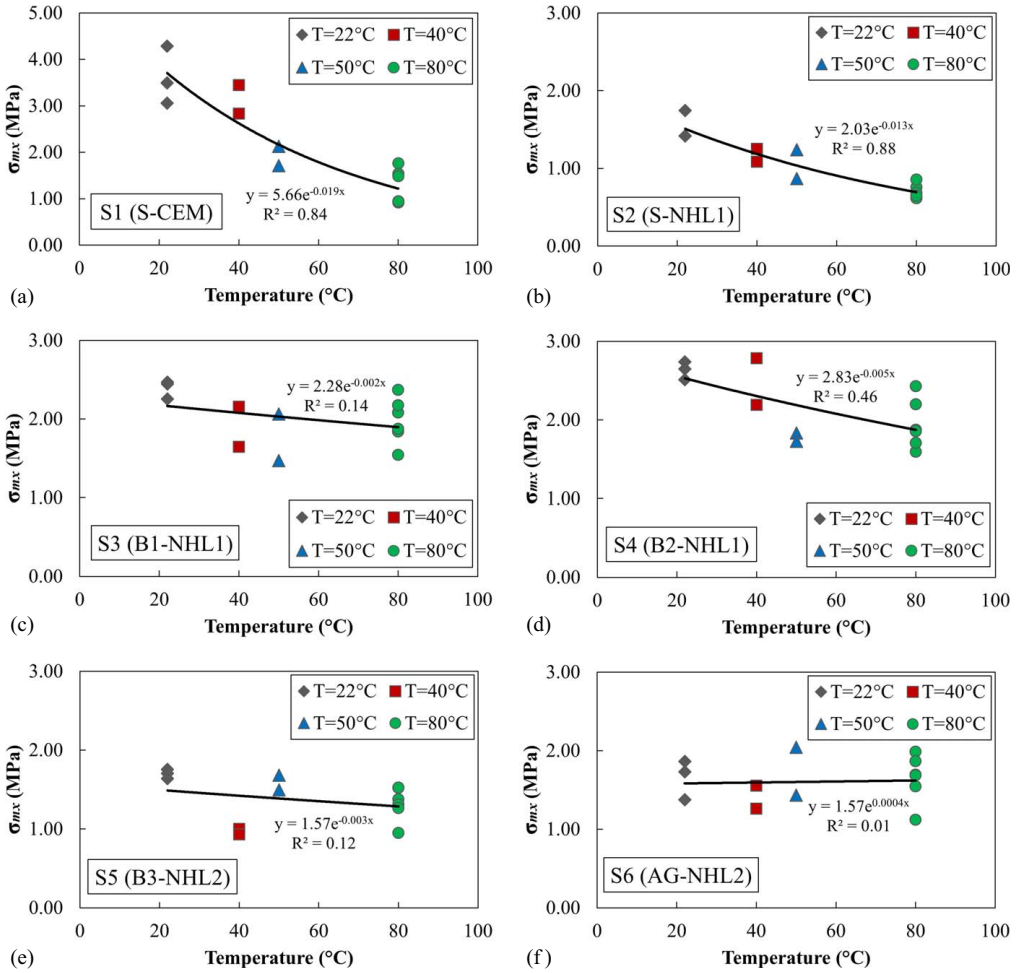

Fig. 14. Tensile stress on the mortar matrix at first cracking versus temperature for the FRCM system: (a) S1 (S-CEM); (b) S2 (S-NHL1); (c) S3 (B1-NHL1); (d) S4 (B2-NHL1); (e) S5 (B3-NHL2); and (f) S6 (AG-NHL2).

Discussion About Qualification Procedures

The performance assessment of FRCM systems subjected to thermal variations was based on a comparison between the results of conditioned and unconditioned samples; this is referred to here as the qualification procedure. The procedure be carried out considering either a "performance" approach, based on a comparison of the results in terms of strength parameters only, or by requiring that the entire tensile response of conditioned FRCM systems be sufficiently close to that of unconditioned ones. In both cases, to qualify an FRCM system for structural purposes, specific ranges with respect to the results of the reference samples should be assigned, within which either the ultimate strength or the stress versus strain curve of the conditioned samples should fall. The qualification procedure for the FRCM systems reported in the Italian guidelines (CSLP 2018) follows the latter approach and prescribes that the average axial stress versus strain curve of the thermally conditioned samples must not deviate more than ±15% from the reference curve, which was the average axial stress versus strain curve of the same FRCM system tested at ambient temperature. In light of the obtained results, and also considering the comparison between average curves for thermally conditioned FRCM systems reported in previous research (Ferretti et al. 2022), it was believed that the comparison between the mechanical properties of conditioned and reference samples should be more focused on the fully cracked phase rather than the initial phases of the tests, thus following a

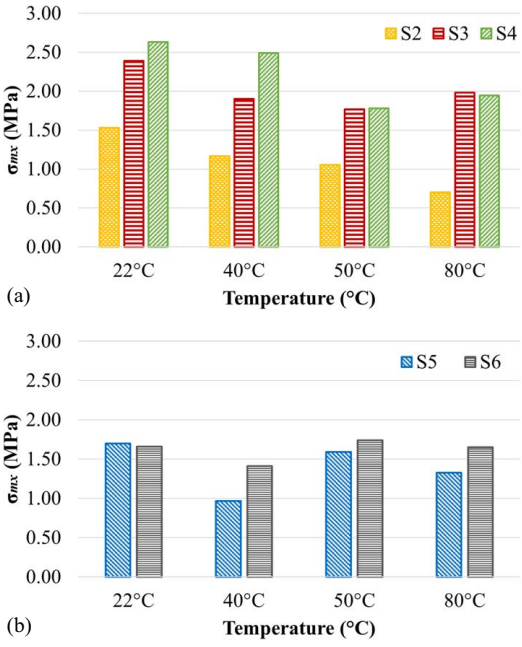

Fig. 15. Comparison between tensile stress on the mortar matrix at first cracking for FRCM systems with (a) mortar matrix NHL1; and (b) mortar matrix NHL2.

performance approach. Indeed, the axial stress and strain values of the cracking phase, which deviated most from the reference results with respect to the values in the fully cracked phase, are not specifically taken into account for design purposes. Therefore, a qualification procedure proposal could be to limit comparisons to the value of the ultimate tensile strength, which should not deviate more than ±15% from the average tensile strength of the reference samples.

Conclusions

The experimental campaign presented in this paper was aimed at studying the effects of thermal variations on the tensile behavior of FRCM systems by performing direct tensile tests on FRCM coupons subjected to different thermal conditioning procedures. The typical trilinear constitutive law characterizing the tensile behavior of FRCM samples was obtained for the conditioned samples; the effect of the applied thermal variations was more evident in the first phases of the tests, that is, the uncracked and the cracking phases. In the fully cracked phase, however, the role of the fibers was prevalent, and the behavior of the samples was not strongly affected by thermal variation.

The effect of temperature in the cracking phase was also studied by computing the stress on the mortar matrix at first cracking, considering the cross-sectional area of the FRCM samples homogenized with respect to the mortar matrix. This stress value was plotted against temperature, which obtained interesting trends for some of the tested FRCM systems, with stress decreasing significantly as the temperature increased. More tests are recommended to better analyze the effect of temperature on mortar matrix behavior, and in considering its composition and the presence of organic components within the mortar mix. It was also observed that the characteristics of the unidirectional and bidirectional fibers influenced the stress at first cracking, depending on their weight density and bundle spacing, on the presence of transversal bundles (bidirectional grids), and on the axial stiffness of the fibers.

The performances of the investigated FRCM systems were also analyzed with reference to the thermal conditioning procedures involving either the use of an oven for the heating phase or the use of a thermal chamber both for heating and testing. Tests showed that when the FRCM coupons were removed from the oven, their temperature decreased quite rapidly due to the thinness of the specimens. Therefore, to reliably evaluate the effect of temperature on FRCM tensile behavior, the use of a thermal chamber for the duration of the tests, both for the heating and the testing phases, is recommended. The exposure period at constant temperature could be reduced with respect to that adopted here for long-term exposure, since no significant differences were observed between samples tested at 80°C with long- or short-term exposure.

Finally, it was suggested that, for qualification purposes, comparisons between the performances of unconditioned and conditioned samples should be limited to the fully cracked phase, since this is the one considered for design purposes.

Even though testing a greater variety of FRCM systems could provide more information regarding the effect of temperature on the first phases of the test (cracking), the study allowed the authors to capture the overall behavior and performances at failure, supporting the robustness of the findings.

Data Availability Statement

All data that support the findings of this study are available from the corresponding author upon reasonable request.

Acknowledgments

The financial support of the Italian Department of Civil Protection (ReLUIS 2021 Grant—Innovative Materials) is gratefully acknowledged. The technical staff at CIRI Buildings & Construction and master's student Abubaker Danfour are gratefully acknowledged for their collaboration during the preparation and execution of the tests.

References

ACI (American Concrete Institute). 2020. *Design and construction of externally bonded Fabric-Reinforced Cementitious Matrix systems for repair and strengthening concrete and masonry structures*. ACI 549.6R-20. Farmington Hills, MI: ACI.

Alecci, V., S. Barducci, A. D'Ambrisi, M. De Stefano, F. Focacci, R. Luciano, and R. Penna. 2019. "Shear capacity of masonry panels repaired with composite materials: Experimental and analytical investigations." *Composites, Part B* 171: 61–69. https://doi.org/10.1016/j.compositesb.2019.04.013.

Ascione, L., G. de Felice, and S. De Santis. 2015. "A qualification method for externally bonded Fibre Reinforced Cementitious Matrix strengthening systems." *Composites, Part B* 78: 497–506. https://doi.org/10.1016/j.compositesb.2015.03.079.

Babaeidarabad, S., F. De Caso, and A. Nanni. 2014. "URM walls strengthened with Fabric-Reinforced Cementitious Matrix composite subjected to diagonal compression." *J. Compos. Constr.* 18 (2): 04013045. https://doi.org/10.1061/(ASCE)CC.1943-5614.0000441.

Bellini, A., M. Bovo, and C. Mazzotti. 2019a. "Experimental and numerical evaluation of fiber-matrix interface behaviour of different FRCM systems." *Composites, Part B* 161: 411–426. https://doi.org/10.1016/j.compositesb.2018.12.115.

Bellini, A., A. Incerti, M. Bovo, and C. Mazzotti. 2018. "Effectiveness of FRCM reinforcement applied to masonry walls subject to axial force and out-of-plane loads evaluated by experimental and numerical studies." *Int. J. Archit. Heritage* 12 (3): 376–394. https://doi.org/10.1080/15583058.2017.1323246.

Bellini, A., S. K. Shahreza, and C. Mazzotti. 2019b. "Cyclic bond behavior of FRCM composites applied on masonry substrate." *Composites, Part B* 169 (March): 189–199. https://doi.org/10.1016/j.compositesb.2019.04.009.

Bellini, A., A. R. Tilocca, I. Frana, M. Savoia, and C. Mazzotti. 2020. "Environmental durability of FRCM strengthening systems and comparison with dry fabrics." In *Proc., 17th Int. Brick and Block Masonry Conf., Brick and Block Masonry – From Historical to Sustainable Masonry*, edited by J. Kubica, A. Kwiecień, and Ł. Bednarz, 987–993. Boca Raton, FL: CRC Press.

Carozzi, F. G., et al. 2017. "Experimental investigation of tensile and bond properties of Carbon-FRCM composites for strengthening masonry elements." *Composites, Part B* 128: 100–119. https://doi.org/10.1016/j.compositesb.2017.06.018.

Ceci, A. M., A. Contento, L. Fanale, D. Galeota, V. Gattulli, M. Lepidi, and F. Potenza. 2010. "Structural performance of the historic and modern buildings of the University of L'Aquila during the seismic events of April 2009." *Eng. Struct.* 32 (7): 1899–1924. https://doi.org/10.1016/j.engstruct.2009.12.023.

CEN (European Committee for Standardization). 2013. *Testing hardened concrete – determination of secant modulus of elasticity in compression*. EN 12390-13. Brussels, Belgium: CEN.

CEN (European Committee for Standardization). 2019. *Methods of test for mortar for masonry – part 11: determination of flexural and compressive strength of hardened mortar*. EN 1015-11. Brussels, Belgium: CEN.

Ceroni, F., G. de Felice, E. Grande, M. Malena, C. Mazzotti, F. Murgo, E. Sacco, and M. R. Valluzzi. 2014. "Analytical and numerical modeling of composite-to-brick bond." *Mater. Struct.* 47 (12): 1987–2003. https://doi.org/10.1617/s11527-014-0382-8.

CSLP (Consiglio Superiore dei Lavori Pubblici). 2018. *Linea guida per la identificazione, la qualificazione ed il controllo di accettazione di compositi fibrorinforzati a matrice inorganica (FRCM) da utilizzarsi per il consolidamento strutturale di costruzioni esistenti*. [In Italian.]. Rome: CSLP.

Dalalbashi, A., B. Ghiassi, and D. V. Oliveira. 2021. "Aging of lime-based TRM composites under natural environmental conditions." *Constr. Build. Mater.* 270: 121853. https://doi.org/10.1016/j.conbuildmat.2020.121853.

D'Ambra, C., G. P. Lignola, A. Prota, F. Fabbrocino, and E. Sacco. 2019. "FRCM strengthening of clay brick walls for out of plane loads." *Composites, Part B* 174: 107050. https://doi.org/10.1016/j.compositesb.2019.107050.

de Felice, G., et al. 2016. "Experimental characterization of composite-to-brick masonry shear bond." *Mater. Struct.* 49 (7): 2581–2596.

Del Gaudio, C., S. A. Scala, P. Ricci, and G. M. Verderame. 2021. "Evolution of the seismic vulnerability of masonry buildings based on the damage data from L'Aquila 2009 event." *Bull. Earthquake Eng.* 19 (11): 4435–4470. https://doi.org/10.1007/s10518-021-01132-x.

Del Zoppo, M., M. Di Ludovico, A. Balsamo, and A. Prota. 2019. "Experimental in-plane shear capacity of clay brick masonry panels strengthened with FRCM and FRM composites." *J. Compos. Constr.* 23 (5): 04019038. https://doi.org/10.1061/(ASCE)CC.1943-5614.0000965.

De Santis, S., et al. 2017. "Round robin test on tensile and bond behaviour of steel reinforced grout systems." *Composites, Part B* 127: 100–120. https://doi.org/10.1016/j.compositesb.2017.03.052.

Donnini, J. 2019. "Durability of glass FRCM systems: Effects of different environments on mechanical properties." *Composites, Part B* 174: 107047. https://doi.org/10.1016/j.compositesb.2019.107047.

Donnini, J., F. De Caso y Basalo, V. Corinaldesi, G. Lancioni, and A. Nanni. 2017. "Fabric-reinforced cementitious matrix behavior at high-temperature: Experimental and numerical results." *Composites, Part B* 108: 108–121. https://doi.org/10.1016/j.compositesb.2016.10.004.

Faella, C., E. Martinelli, E. Nigro, and S. Paciello. 2010. "Shear capacity of masonry walls externally strengthened by a cement-based composite material: An experimental campaign." *Constr. Build. Mater.* 24 (1): 84–93. https://doi.org/10.1016/j.conbuildmat.2009.08.019.

Ferretti, F., A. Incerti, A. R. Tilocca, and C. Mazzotti. 2021. "In-plane shear behavior of stone masonry panels strengthened through grout injection and fiber reinforced cementitious matrices." *Int. J. Archit. Heritage* 15 (10): 1375–1394. https://doi.org/10.1080/15583058.2019.1675803.

Ferretti, F., and C. Mazzotti. 2021. "FRCM/SRG strengthened masonry in diagonal compression: Experimental results and analytical approach proposal." *Constr. Build. Mater.* 283: 122766. https://doi.org/10.1016/j.conbuildmat.2021.122766.

Ferretti, F., A. R. Tilocca, A. Incerti, C. Mazzotti, and M. Savoia. 2022. "Tensile behavior of FRCM coupons under thermal stresses." *Key Eng. Mater.* 916: 50–57. https://doi.org/10.4028/p-rki9n6.

Incerti, A., F. Ferretti, and C. Mazzotti. 2019. "FRCM strengthening systems efficiency on the shear behavior of pre-damaged masonry panels: An experimental study." *J. Build. Pathol. Rehabil.* 4 (1): 14. https://doi.org/10.1007/s41024-019-0053-9.

Incerti, A., A. Vasiliu, B. Ferracuti, and C. Mazzotti. 2015. "Uni-axial compressive tests on masonry columns confined by FRP and FRCM." In *Proc., 12th Int. Symp. on Fiber Reinforced Polymers for Reinforced Concrete Structures & 5th Asia-Pacific Conference on Fiber Reinforced Polymers in Structures Joint Conference*, edited by Z. Wu, G. Wu, and X. Wang, 14–16. Dhaka, Bangladesh: Southeast Univ.

Iorfida, A., S. Candamano, F. Crea, L. Ombres, S. Verre, and P. de Fazio. 2019. "Bond behaviour of FRCM composites: Effects of high temperature." *Key Eng. Mater.* 817: 161–166. https://doi.org/10.4028/www.scientific.net/KEM.817.161.

Lagomarsino, S. 2006. "On the vulnerability assessment of monumental buildings." *Bull. Earthquake Eng.* 4 (4): 445–463. https://doi.org/10.1007/s10518-006-9025-y.

Leone, M., et al. 2017. "Glass fabric reinforced cementitious matrix: Tensile properties and bond performance on masonry substrate." *Composites, Part B* 127: 196–214. https://doi.org/10.1016/j.compositesb.2017.06.028.

Lignola, G. P., et al. 2017. "Performance assessment of basalt FRCM for retrofit applications on masonry." *Composites, Part B* 128: 1–18. https://doi.org/10.1016/j.compositesb.2017.05.003.

Marcari, G., M. Basili, and F. Vestroni. 2017. "Experimental investigation of tuff masonry panels reinforced with surface bonded basalt textile-reinforced mortar." *Composites, Part B* 108: 131–142. https://doi.org/10.1016/j.compositesb.2016.09.094.

Maroudas, S. R., and C. C. G. Papanicolaou. 2017. "Effect of high temperatures on the TRM-to-masonry bond." *Key Eng. Mater.* 747: 533–541. https://doi.org/10.4028/www.scientific.net/KEM.747.533.

Micelli, F., and M. A. Aiello. 2019. "Residual tensile strength of dry and impregnated reinforcement fibres after exposure to alkaline environments." *Composites, Part B* 159: 490–501. https://doi.org/10.1016/j.compositesb.2017.03.005.

Mininno, G., B. Ghiassi, and D. V. Oliveira. 2017. "Modelling of the in-plane and out-of-plane performance of TRM-strengthened masonry walls." *Key Eng. Mater.* 747: 60–68. https://doi.org/10.4028/www.scientific.net/KEM.747.60.

Ministero delle Infrastrutture e dei Trasporti. 2018. *Aggiornamento delle 'Norme Tecniche per le Costruzioni'*, 1–198. [In Italian.] Rome: Gazzetta Ufficiale della Repubblica Italiana.

Murgo, F. S., F. Ferretti, and C. Mazzotti. 2021. "A discrete-cracking numerical model for the in-plane behavior of FRCM strengthened masonry panels." *Bull. Earthquake Eng.* 19 (11): 4471–4502. https://doi.org/10.1007/s10518-021-01129-6.

Nobili, A., and C. Signorini. 2017. "On the effect of curing time and environmental exposure on impregnated Carbon Fabric Reinforced Cementitious Matrix composite with design considerations." *Composites, Part B* 112: 300–313. https://doi.org/10.1016/j.compositesb.2016.12.022.

Oliveira, D. V., R. A. Silva, E. Garbin, and P. B. Lourenço. 2012. "Strengthening of three-leaf stone masonry walls: An experimental research." *Mater. Struct.* 45 (8): 1259–1276. https://doi.org/10.1617/s11527-012-9832-3.

Ombres, L., A. Iorfida, S. Mazzuca, and S. Verre. 2018. "Bond analysis of thermally conditioned FRCM-masonry joints." *Measurement* 125: 509–515. https://doi.org/10.1016/j.measurement.2018.05.021.

Papanicolaou, C. G., T. C. Triantafillou, M. Papathanasiou, and K. Karlos. 2007. "Textile reinforced mortar (TRM) versus FRP as strengthening material of URM walls: Out-of-plane cyclic loading." *Mater. Struct.* 41 (1): 143–157. https://doi.org/10.1617/s11527-007-9226-0.

Parisi, F., I. Iovinella, A. Balsamo, N. Augenti, and A. Prota. 2013. "In-plane behaviour of tuff masonry strengthened with inorganic matrix–grid composites." *Composites, Part B* 45 (1): 1657–1666. https://doi.org/10.1016/j.compositesb.2012.09.068.

Penna, A. 2015. "Seismic assessment of existing and strengthened stone-masonry buildings: Critical issues and possible strategies." *Bull. Earthquake Eng.* 13 (4): 1051–1071. https://doi.org/10.1007/s10518-014-9659-0.

Shrive, N. G. 2006. "The use of fibre reinforced polymers to improve seismic resistance of masonry." *Constr. Build. Mater.* 20 (4): 269–277. https://doi.org/10.1016/j.conbuildmat.2005.08.030.

Valluzzi, M. R. 2016. "Challenges and perspectives for the protection of masonry structures in historic centers: The role of innovative materials and techniques." *RILEM Tech. Lett.* 1: 45. https://doi.org/10.21809/rilemtechlett.2016.10.

Valluzzi, M. R., et al. 2012. "Round Robin Test for composite-to-brick shear bond characterization." *Mater. Struct.* 45 (12): 1761–1791. https://doi.org/10.1617/s11527-012-9883-5.